Simulation of electromagnetic fields of Terahertz Antennas using CST Studio™

Eloi Canals and Jaume Villasante
Projects of Engineering Physics 2. Universitat Politècnica de Catalunya
(Dated: June 19, 2020)

The so-called 'terahertz gap', which ranges from 0.3 to 10 THz, is the last span within the whole electromagnetic wave spectrum that has not been technologically or commercially developed. This frequency range has remarkable properties for many applications, such as medical imaging, communication or security systems. The major advantages of terahertz waves is that many materials appear to be transparent in that spectral region and it is harmless for biological entities.
In wireless communication systems, terahertz technology allows a faster transmission of information than the current microwave technology. There is therefore an increasing need to design antennas which can radiate in the region of the terahertz gap. CST Studio™ is a program that allows to design such antennas and simulate their radiation pattern.
The aim of this report is to show how Alessandro Garufo, Giorgio Carluccio, Nuria Llombart, and Andrea Neto designed and obtained the electromagnetic fields of the dipolar, spiral and Sierpinski antennas.

I. INTRODUCTION

Photoconductive antennas (or PACs) are nowadays the most commonly used devices to generate terahertz waves. These antennas consist of a semiconductor substrate (usually GaAs) which provides the electron current that will generate the pulse. PCAs can be used as a THz transmitter as well as THz receiver. In case of a transmitter, a femto-second pulsed laser is aimed at a small gap between two metallic parts that are held at a certain bias voltage through some electrodes. The light generates electron-hole pairs which are accelerated by the bias voltage. The antenna behaves like a Hertzian dipole and radiates consequently terahertz waves. In case of a THz receiver, an amplifier is connected on the electrical contacts. During the optical pulse the excited carriers are accelerated by the electric field component of the incident THz pulse. This leads to a voltage signal across the gap of the antenna.

A. Hyperhemispherical lenses

The waves produced by the antenna reflect at the interface between the substrate and the propagation medium (in our case, the air). In order to avoid losing part of the generated electromagnetic radiation due to total reflection, silicon hyperhemispherical lenses are used.

The maximum incident angle has to be smaller than the critical angle, thus one can impose some conditions on the dimensions of the lens.

$$n_i \sin(\theta_i) = n \sin(\theta_c) \Rightarrow \sin(\theta_c) = \frac{1}{n} \tag{1}$$

As can be seen in Figure 1, the maximum angle of incidence is related to the dimensions of the lens by $\sin(\theta_{max}) = \frac{L}{R}$. Therefore,

$$\boxed{\theta_{max} \leq \theta_c \Rightarrow L \leq \frac{R}{n}} \tag{2}$$

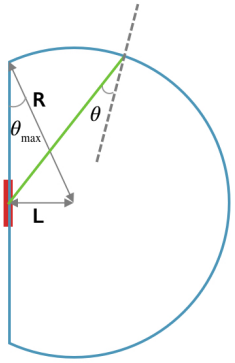

FIG. 1. Schematic representation of the parameters of the lens.

II. SIMULATIONS

A. Dipolar antenna

Let us begin the batch of simulations with the dipole antenna, the simplest one. For that purpose, a file with the dipole antenna features is provided. CST allows countless of configurations in terms of boundaries, the background the antenna should have, the procedure of simulation itself... In our particular case, the domain and asymptotic solvers are the ones primarily used, and the boundaries correspond to YZ plane (magnetic field=0) and XZ plane (electric field=0). There is also a possibility to set a decoupling plane in case the calculation domain is intersected by a metallic plane which is supposed to extend to infinity. One might experiment the position of this plane can yield a number of different scenarios, some of which are better than others. Its implementation is controversial in the scientific community, as can be seen in the papers [1] and [2]. Nevertheless, we keep it without decoupling plane and try later several values at different z to see which configuration is more realistic

together with a current-type port located at the middle of the gap. The results obtained using the time domain solver are shown in Figure 3 and 4 for two possible values of the antena air box, $15\mu m$ and $5\mu m$.

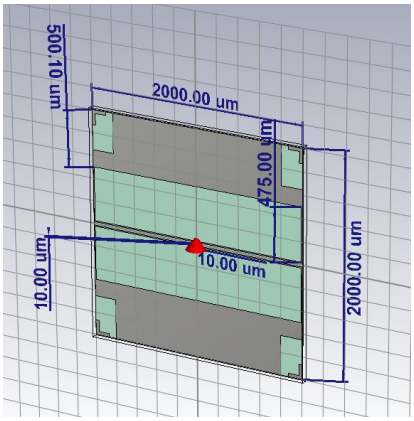

FIG. 2. Structure of the dipolar antenna with its dimensions.

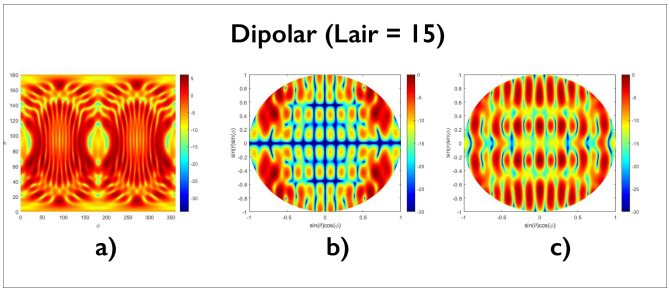

FIG. 3. 2D plots of the simulated dipolar radiation patterns, with $L_{\text{air}} = 15\mu m$, corresponding to a) abs b) X-polarization c) Co-polarization. Frequency 0.3THz.

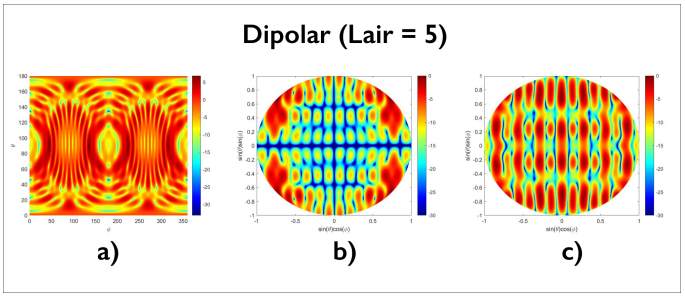

FIG. 4. 2D plots of the simulated dipolar radiation patterns with $L_{\text{air}} = 5\mu m$, corresponding to a) abs b) X-polarization c) Co-polarization. Frequency 0.3THz.

Now we are interested in finding out what is the effect that the addition of a decoupling plane has. For this reason, we plot for both dipolar antennas the corresponding co-polarizations because it is the one that shows the radiation in the desired direction as opposed to the X-polarization, which shows the dissipation.

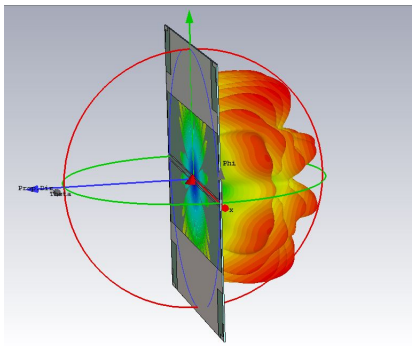

FIG. 5. CST radiation pattern for a decoupling plane located at $Z = 18\mu m$

Upon testing different values we came to the conclusion that the difference that the inclusion of a decoupling plane makes is almost unnoticeable. However, for a decoupling plane higher than $Z = 17\mu m$ in both cases, the antenna only radiates towards negative z direction (Figure 5). This makes sense due to the fact that the decoupling plane attenuates the radiation from the origin to the position of this plane. In our case, the designed parameters of the antenna causes all the radiation to be concentrated on the other side of the plane.

B. Spiral antenna

A problem arised when simulting this antenna, namely that our license is limited by the so-called cells per wavelength. Increasing the mesh lines per wavelength increases the mesh cell count and simulation time and thus the accuracy. The issue is that our student's license doesn't support much cells and therefore we had to cut back the frequency to the lowest value the CST offers, 0.3THz. This antenna is built using a default macro of CST. There are many options to build spirals, but we chose the logarithmic spiral one and played with the different parameters to reach the structure seen in Figure 6.

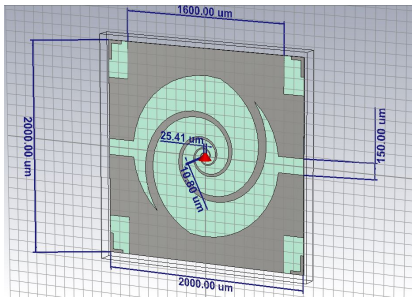

FIG. 6. Structure of spiral antenna with its dimensions.

To better understand the effect of the hyperhemispherical lens, we simulated a more realistic case in which the background of the antenna was air (n = 1). This creates

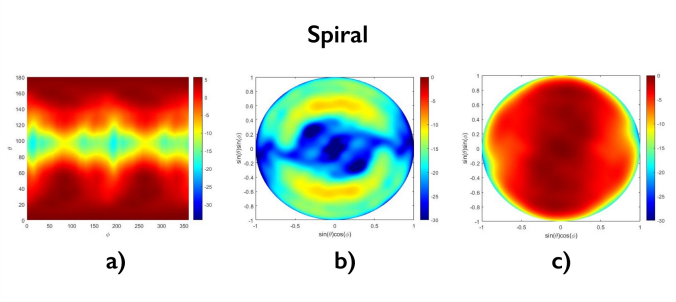

FIG. 7. 2D plots of the simulated spiral radiation patterns without the lens, corresponding to a) abs b) left circular polarization c) right circular polarization. Frequency 0.3THz.

a boundary between the substrate and the air with different index of refraction and accordingly radiated light will experience reflections, disturbing the radiation pattern. From the right circular polarization pattern of Figure 8, it can be noted that the radiation undergoes a rotation along the propagation direction.

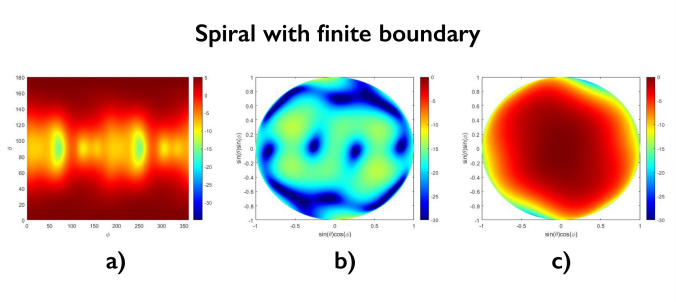

FIG. 8. 2D plots of the simulated spiral radiation patterns with a finite substrate, corresponding to a) abs b) left circular polarization c) right circular polarization. Frequency 0.3THz.

To generate the electromagnetic fields of the spiral antenna with the lens, we first exported the data from the spiral with infinite substrate as a farfield. Then we selected that farfield as the source for the lens file, instead of defining a port. It was not possible to simulate the fields using the integral solver due to the problem of the maximum mesh cells. Therefore, we simulated the fields with the asymptotic solver, which does not support boundaries. For this reason, the selected farfield was the one with infinite substrate and not the one with boundaries as one would expect. Rather than simulating the radiation pattern of a more realistic case, we compared the effect of the lens on the ideal case. As shown in Figure 9 and Figure 7, the radiation patterns are nearly exact. This is the result we expected, as the lens prevents total reflection to the substrate and in the case of infinite substrate there is no reflection.

Due to the fact that the time domain solver requires an input port and the excitation in this case consists in a farfield as source, there was a need to use asymptotic or integral when considering the lense. The integral was problematic because our license is limited to 2000 mesh cells and as commented previously even when reducing all settings to minimum its implementation was not possible. As a result of this circumstance, the asymptotic solver was used.

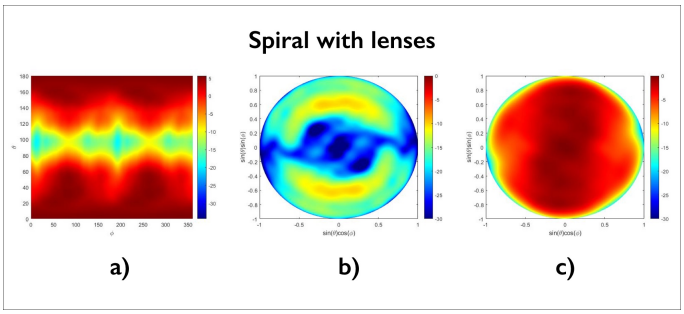

FIG. 9. 2D plots of the simulated spiral radiation patterns with the lens, corresponding to a) abs b) left circular polarization c) right circular polarization. Frequency 0.3THz.

C. Sierpinski antenna

In order to build this antenna in CST, we used a macro that constructed the characteristic Sierpinski fractal. After that, we mirrored the object so that it took the form of an antenna and removed those parts that were in contact with the gap using boolean operations. By changing the parameters of the antenna we could also change the number of triangles generated by the Sierpinski macro (changing the Sierpinski iterations parameter), thus giving different radiation behaviour. The macro is not perfectly optimized and sometimes gives errors, but the final function fulfills it satisfactorily.

Once the structure of the antenna was built, we defined a discrete current port located in the middle of the gap and made sure that it was in contact with the metallic parts. We built afterwards the air box and the GaAs substrate and simulated the radiation patterns with the time domain solver.

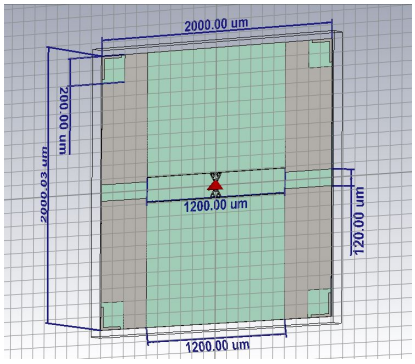

FIG. 10. Structure of the Sierpisnki antenna with its dimensions.

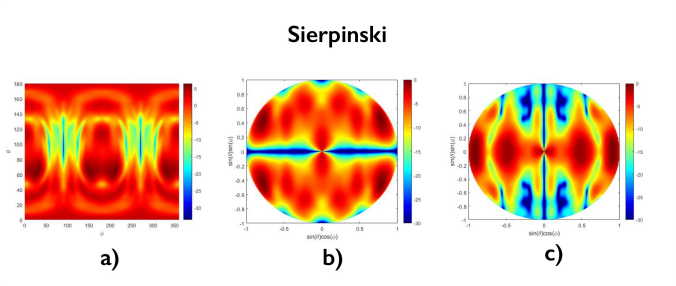

FIG. 11. 2D plots of the simulated Sierpinski radiation patterns, corresponding to a) abs b) X-polarization c) Co-polarization. Frequency 0.3THz. Sierpinski parameter: 4.

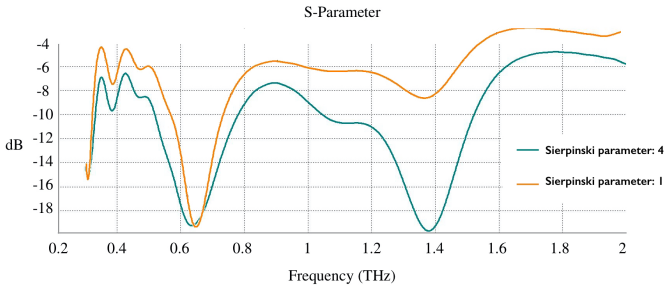

FIG. 12. S-parameter of the Sierpinski antenna ranging from 0.2 to 2 THz for Sierpinski parameter: 4 and 1.

Sierpinski antennas show a multiband behaviour that is based on the self-similarity properties of the antenna's fractal shape, which might open an alternative way for designing new multiband and frequency independent antennas.

One important characteristic parameter of an antenna is the S-parameter. In particular, the S11 parameter represents how much power is reflected from the antenna, and for that reason is known as the reflection coefficient. 0dB means that nothing is radiated and all power is reflected from the antenna. As it can be seen in Figure 12, the antenna shows a resonance at $\sim 0.6THz$ and another one at $\sim 1.4THz$ for a Sierpinski parameter equal to 4, meaning that it can radiate at both frequencies.

When number of Sierpinski fractals generated decreases, the resonance at the frequency of $1.4THz$ also decreases, so it no longer behaves as a multiband antenna. In Figure 12, one can see this effect with the Sierpinski parameter equal to 1.

III. DISCUSSION

The data must be exported in ASCII format when using the software in order to observe the radiation diagrams. Note that one must select whether the radiation is linear, as in the case of the dipole, or circular, as in the case of the spiral. After that, the data is treated with a Matlab code to draw the radiation graphs. We had to do some adjustments to the code that M. Roigé [3] used as well as modifying the proper step size of the own data in CST, due to the fact that our data resolution was not the same.

Although due to the limitations of the student licenses it was not possible to simulate at all the desired frequencies, the diagrams obtained with this procedure are incredibly similar to the ones obtained by A. Garufo, N. LLobrat, G. Carluccio and A. Neto in their paper [1].

IV. CONCLUSION

The main goal of this project was to understand how to simulate different antennas and more specifically get a broader insight of the bandwidth of THz. In the relatively short available time we have gained an understanding on how tricky and complex this whole world can be. In particular, we observed how changing different parameters can lead to slightly different outcomes. CST can offer a wide range of possibilities due to the large potential it has. We come to the conclusion that it is a very suitable option to simulate, among other purposes, THz antennas.

ACKNOWLEDGEMENTS

Not only we have acquired knowledge, but also, and more importantly, we have been able to apply it with our own hands, with the entailing satisfaction that this fact has provided us. We are now aware of the complications and difficulties of the entire process in addition to the relevance and utility such procedure grants.

Last but not least, we also want to express our gratitude to Conchi and Cristian for their patience and devotion.

[1] A. Garufo, G. Carluccio, J. R. Freeman, D. R. Bacon, N. Llombart, E. H. Linfield, A. G. Davies, and A. Neto. Norton equivalent circuit for pulsed photoconductive antennas—part ii: Experimental validation.

[2] A. Garufo, N. Llombart, and A. Neto. Norton equivalent circuit for pulsed photoconductive antennas–part i: Theoretical model. April 2018.

[3] Miquel Roigé Llop. Experimentos con ondas de terahercios. Barcelona, January 2020.

Appendix A: Matlab code to generate radiation diagrams

```
clear
close all
load('dddipolar.txt', '-ascii')
a=dddipolar;

% radiation pattern choice
% rp=3 abs, rp=4 Xpol, rp=6 copol
b=a(:,6);
t=linspace(0,180,361);
p=linspace(0,360,721)
tr=t*pi/180;
pr=p*pi/180;
c=reshape(b,length(t),length(p)-1);
d=[c,c(:,1)];
%normalized to zero dB
dm=max(max(d))
e=d-dm;

%avoiding negative values
ss=min(min(d));
if ss>0
    ss=0
end

f=d+abs(ss);

x1=sin(tr')*cos(pr);
y1=sin(tr')*sin(pr);
z1=cos(tr')*ones(size(pr));

x2=f.*x1;
y2=f.*y1;
z2=f.*z1;

% to plot only the positive z fields

tr2=tr(1:90);

x12=sin(tr2')*cos(pr);
y12=sin(tr2')*sin(pr);


figure(1)
colormap('jet')
h=pcolor(p,t,d)
caxis([-40+dm dm])
set(h,'edgecolor','none')
colorbar
xlabel('\phi')
ylabel('\theta')

figure(2)
colormap('jet')
h=pcolor(x12,y12,e(1:90,:))
caxis([-30 0])
set(h,'edgecolor','none')
xlabel('sin(\theta)cos(\phi)')
ylabel('sin(\theta)sin(\phi)')
colorbar
```